Enhancement of Hemodynamic Contrast in the Cancerous Breast by Controlled Articulation

Rabah Al abdi[1,4]; Harry L. Graber[1,2]; Christoph H. Schmitz[2,3]; Randall L. Barbour[1,2]

[1]SUNY Downstate Medical Center, Brooklyn, NY, USA; [2]NIRx Medizintechnik GmbH, Berlin, DEU;
[3]NIRx Medical Technologies, Glen Head, NY, USA; [4]Jordan University of Science and Technology, Irbid, JOR

INTRODUCTION

Details of blood delivery to tissue and bulk fluid redistribution among the various tissue compartments frequently are impacted by disease or trauma. For example, derangements in hemodynamic states, accompanied by increased tissue stiffness and local edema, is a common breast cancer phenotype [1]. Accordingly, we have hypothesized that externally applied mechanical forces can produce distinct dynamic responses between diseased and healthy tissues, thereby enhancing diagnostic image contrast. Additional evidence for this sort of contrast-enhancing effect comes from correspondences that we have observed between fNIRS-based hemodynamic image data and results of computed estimates of internal mechanical stress and pressure distributions, as a function of various applied articulation maneuvers [2]. The latter suggest that spatial distributions of hemodynamic variables in the fNIRS images represent redistributions of blood in response to changes in the internal stress. Here we present results from a pre-clinical study that we have conducted, using a recently developed an fNIRS-based breast imaging system [3], to evaluate the hypothesis that image contrast between breast tumors and surrounding healthy tissue may be enhanced via controlled articulation maneuvers.
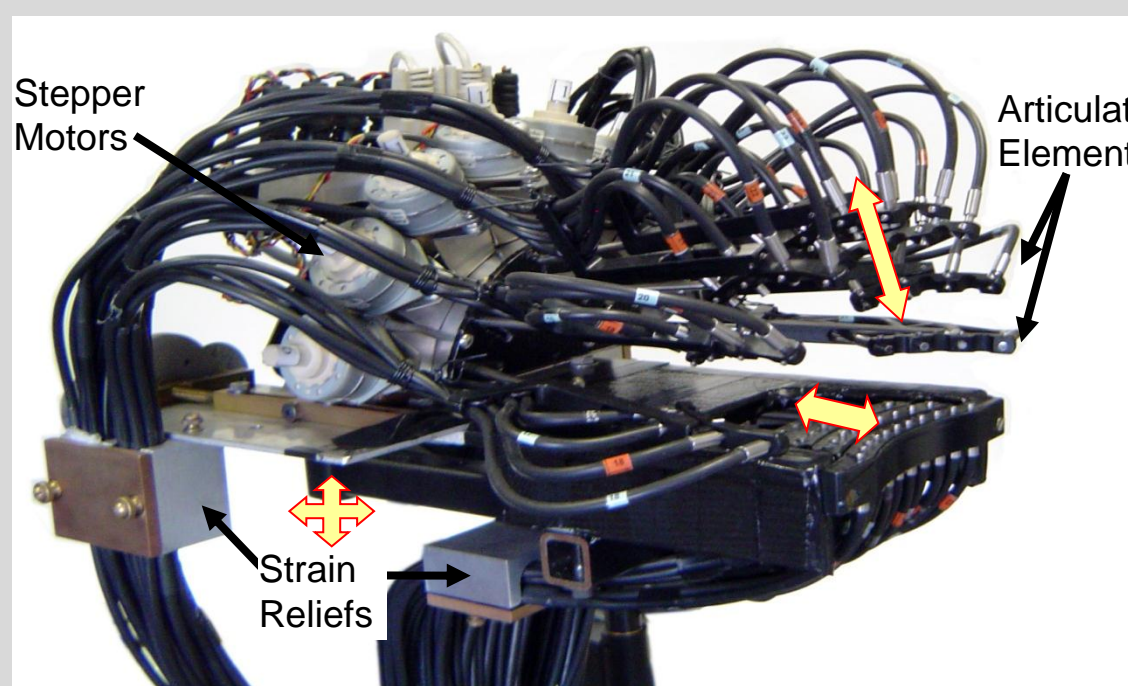
INSTRUMENTATION

Fig. 1.: A photograph of one of the left-breast sensing head. The right-breast sensing head is a mirror image of the one shown.
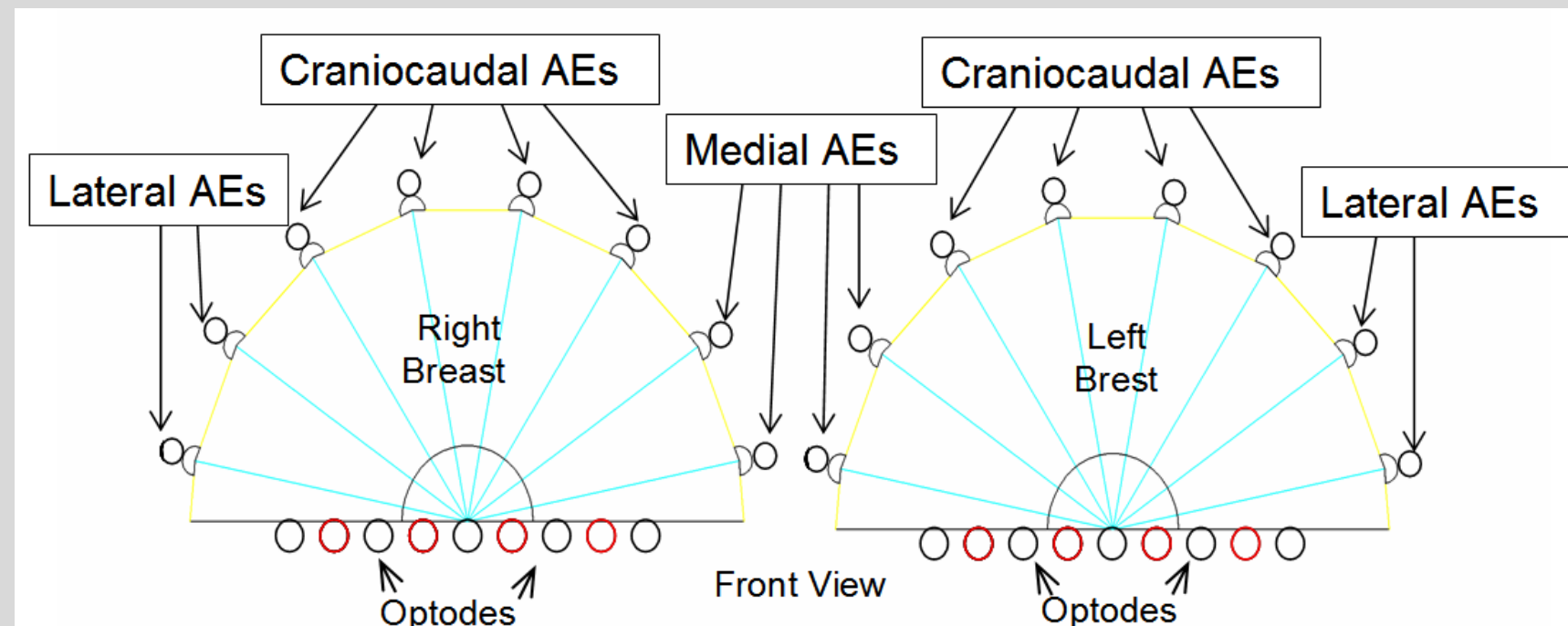

Fig. 2. A schematic of the location of the articulating elements (AEs) relative to the left and right breasts. Each AE can be controlled separately. This enabled us to explore the impact of force magnitude and of the articulation protocol—compression with all AEs, or with only craniocaudal (CC) or only mediolateral (ML) AEs, or oscillatory or wavelike patterns—on diagnostic accuracy.
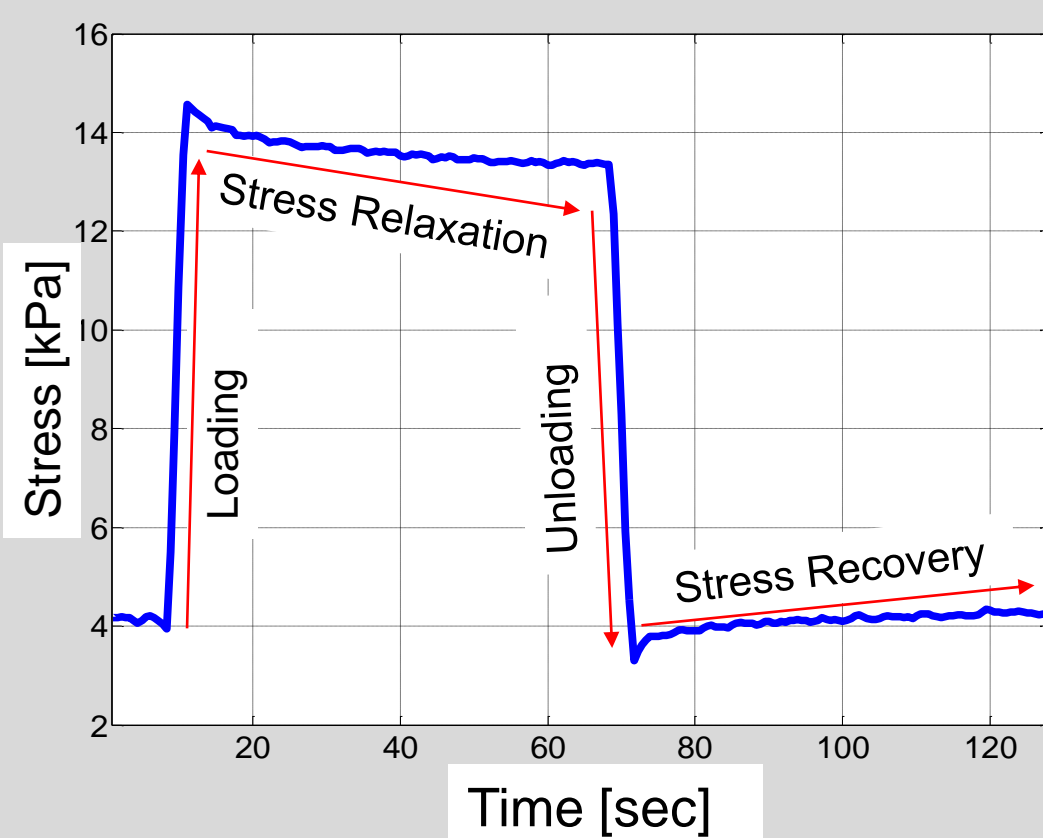
EXPERIMENTAL PROTOCOL AND STUDY POPULATION

Fig. 3. The four phases of a quasi-static compression protocol.

Group	Number	Age (yrs)	BMI
Cancer	17	55.7 ±10.5	33.4 ± 8.1
Benign	21	49.9 ± 9. 4	32.0 ± 6.1
Healthy	24	54.3 ± 12.1	30.1 ± 4.3

Table 1. Patients' clinical information. Among the 17 subjects with active breast cancer at the time of examination, there were 11 cases of invasive ductal carcinoma (IDC), 2 of invasive mammary carcinoma (IMC), 2 of ductal carcinoma in situ (DCIS), and 2 of intraductal carcinoma (IC). Tumor dimensions ranged from 0.5 cm to 6 cm.

Following a five-minute baseline scan, the skin-optode contact pressure was rapidly (~2 s) increased to a level of either 4.4 N or 7.1 N, and data collection continued during the subsequent period of stress relaxation (60-120 s). Optical data were analyzed offline: application of a low-pass filter with a 0.2-Hz cutoff frequency was followed by use of the Normalized Difference Method to reconstruct images of oxygenated and deoxygenated hemoglobin (HbO, HbD), tissue oxygen saturation (HbSat), and blood volume (HbT) [4].

Fig. 4. Mechanical articulations introduce optical pathlength changes, producing large changes in optical signal that do not represent true hemodynamic variations. To minimize this effect, all hemodynamic-response results presented below were computed from data collected 30-55 seconds after the end of the relevant change in AE positions (e.g., stress- relaxation results are derived from data 30-55 s after the end of the loading phase (see Fig. 3)).
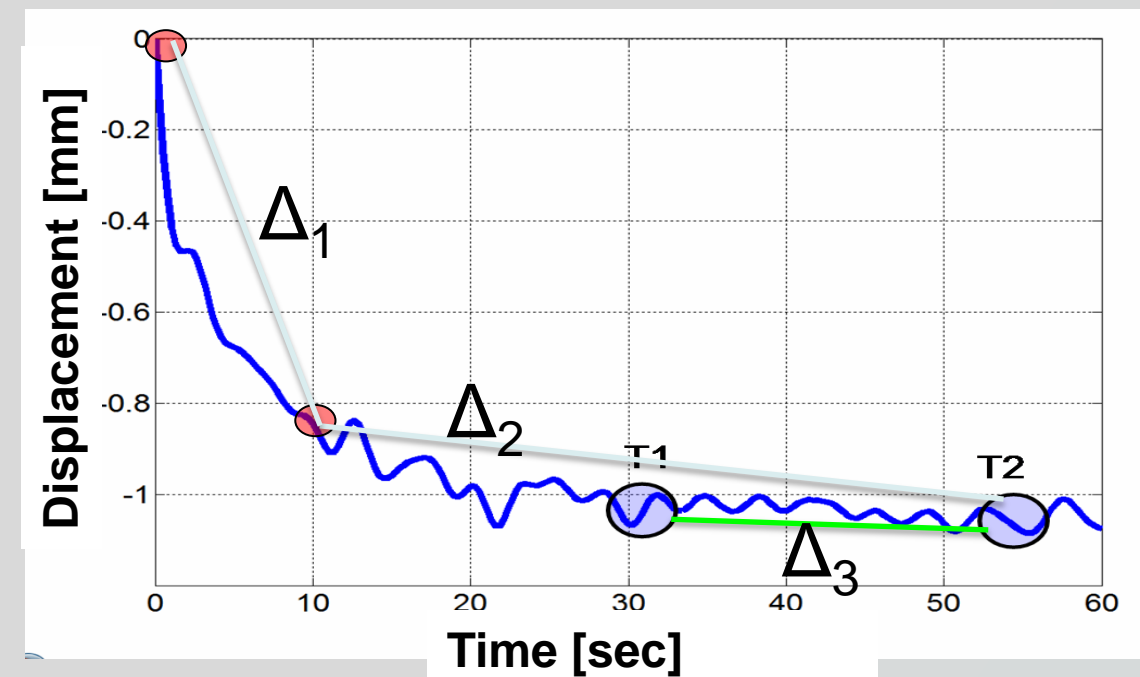
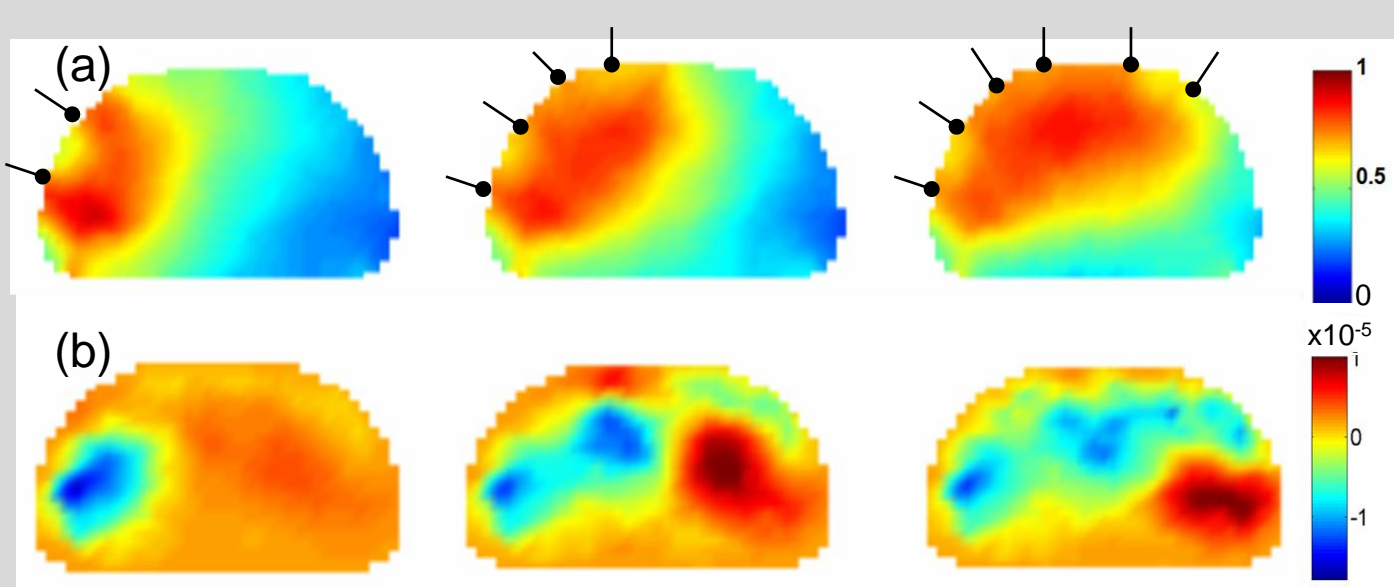## INDIVIDUAL Hb SIGNAL COMPONENT RESULTS

Fig. 5. (a) Spatial distributions of effective stress calculated [2] for a wave-like compression proceeding from left to right, where black markers indicate the active articulating elements. For the computations, the breast was modeled as consisting of a homogeneous poro-eleastic material. (b) Reconstructed images of HbT, for a healthy subject (43 year-old woman with D breast size and BMI of 35) who underwent the same pattern of progressive compression as was used for the model computations.
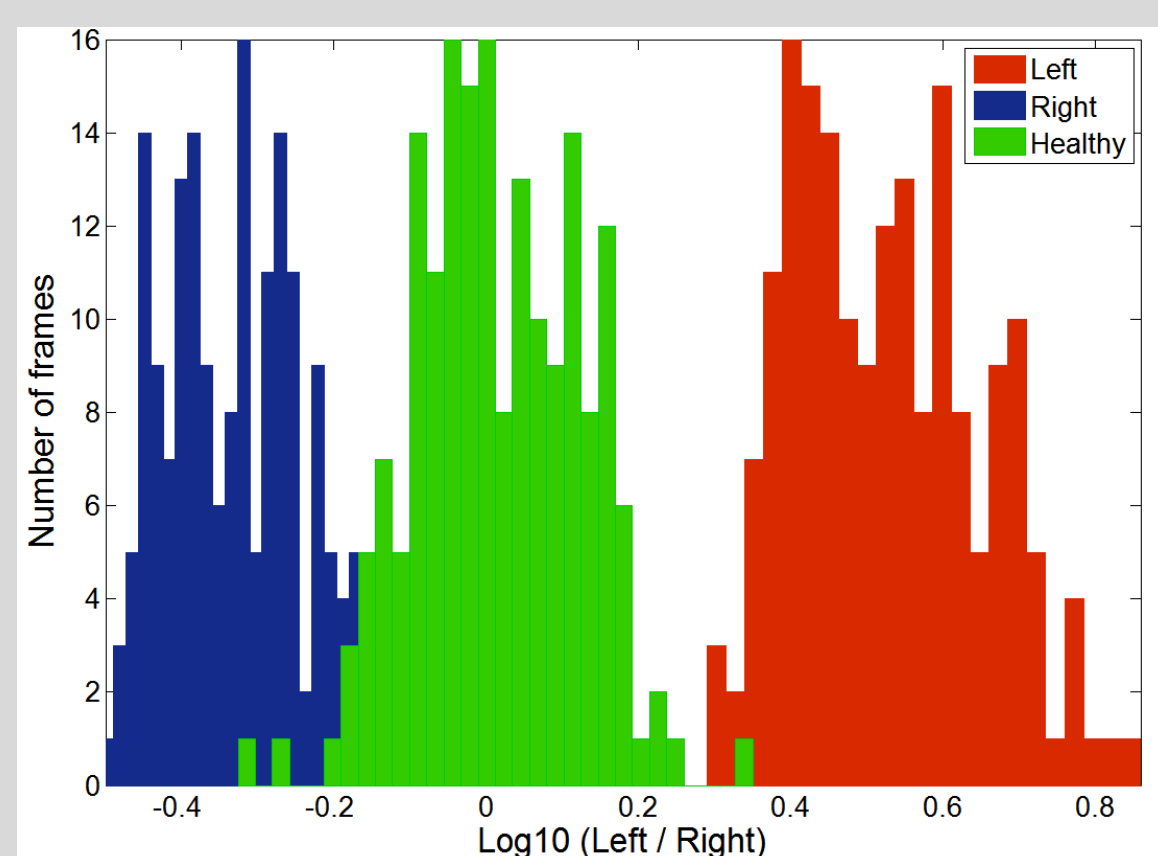

Fig. 6. Demonstration of pathology-dependent inter-breast differences. Subjects are 56 y/o with 2-cm DCIS in the left breast (red), 36 y/o with 1-cm IDC in the right breast (blue), and 59 y/o healthy control (green). Data considered are HbD (similar findings are obtained for all components of the Hb signal) time series, for both breasts, recovered from data collected during the stress relaxation time segment (Fig. 3). For each time frame, the standard deviation (SD) of HdD values across the entire breast (SSD = spatial SD) was computed. As an index of inter-breast difference, we subsequently computed $A = \log_{10}(SSD_{left}/SSD_{right})$; the null hypothesis is that values of A should cluster about 0. The plotted histograms indicate the numbers of time frames for which each A value was obtained, for each subject. The A values for the breast-cancer subjects indicate substantially larger SSD in the affected breast, while the healthy subject's data conform to the null hypothesis.
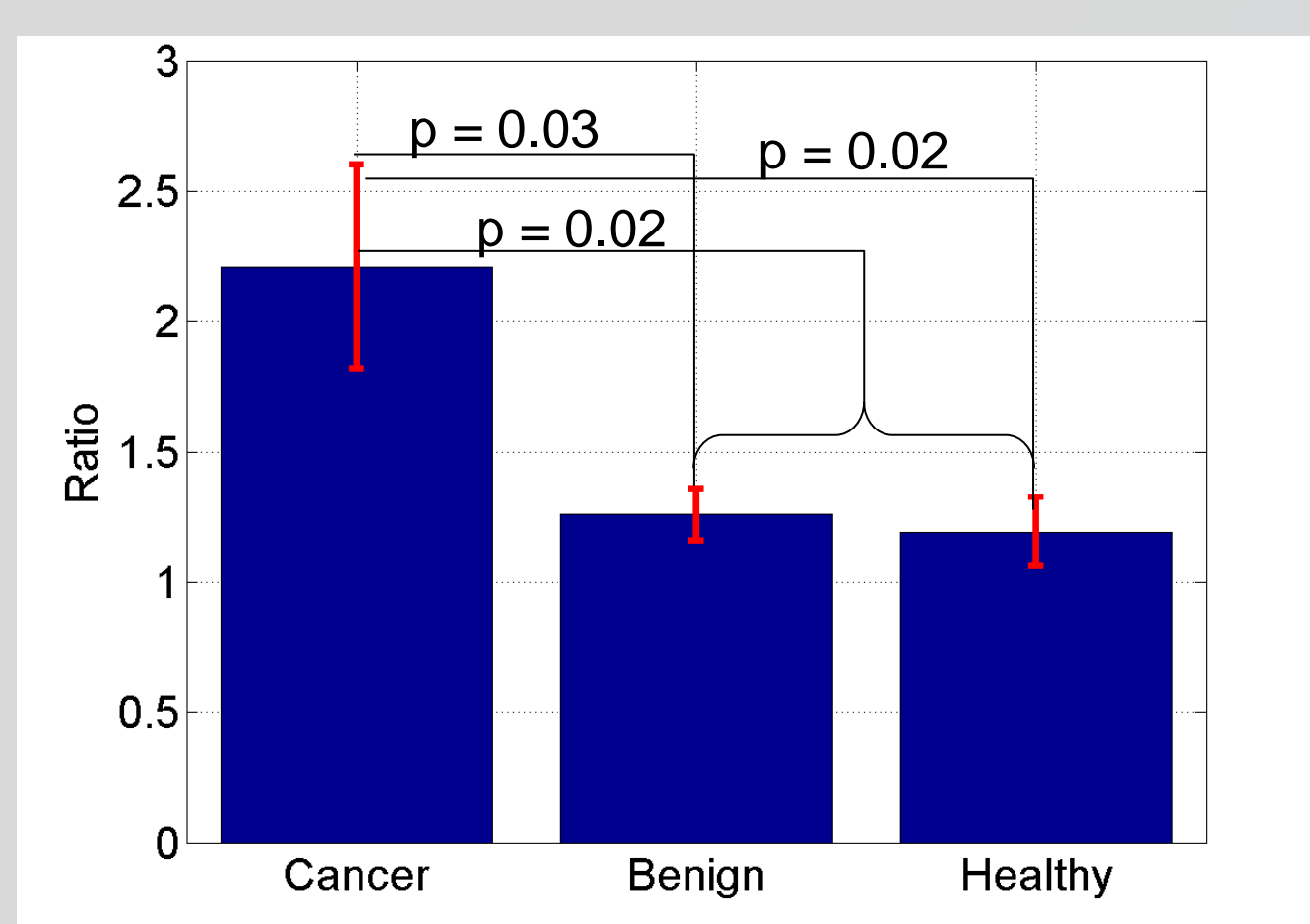

Fig. 7. Group means and standard errors for inter-breast SSD ratios, derived from HbD (similar findings are obtained for all components of the Hb signal) concentrations recovered from data collected during force relaxation following an ML compression. The computed ratio is SSD_{left}/SSD_{right} for healthy subjects, and $SSD_{affected}/SSD_{unaffected}$ for subjects with known pathologies. As indicated, the mean inter-breast ratio for the breast-cancer group is larger than that for the other two groups by a statistically significant amount. However, the difference is not sufficiently large to permit use of the SSD ratio as a diagnostic metric of breast cancer in individual cases.

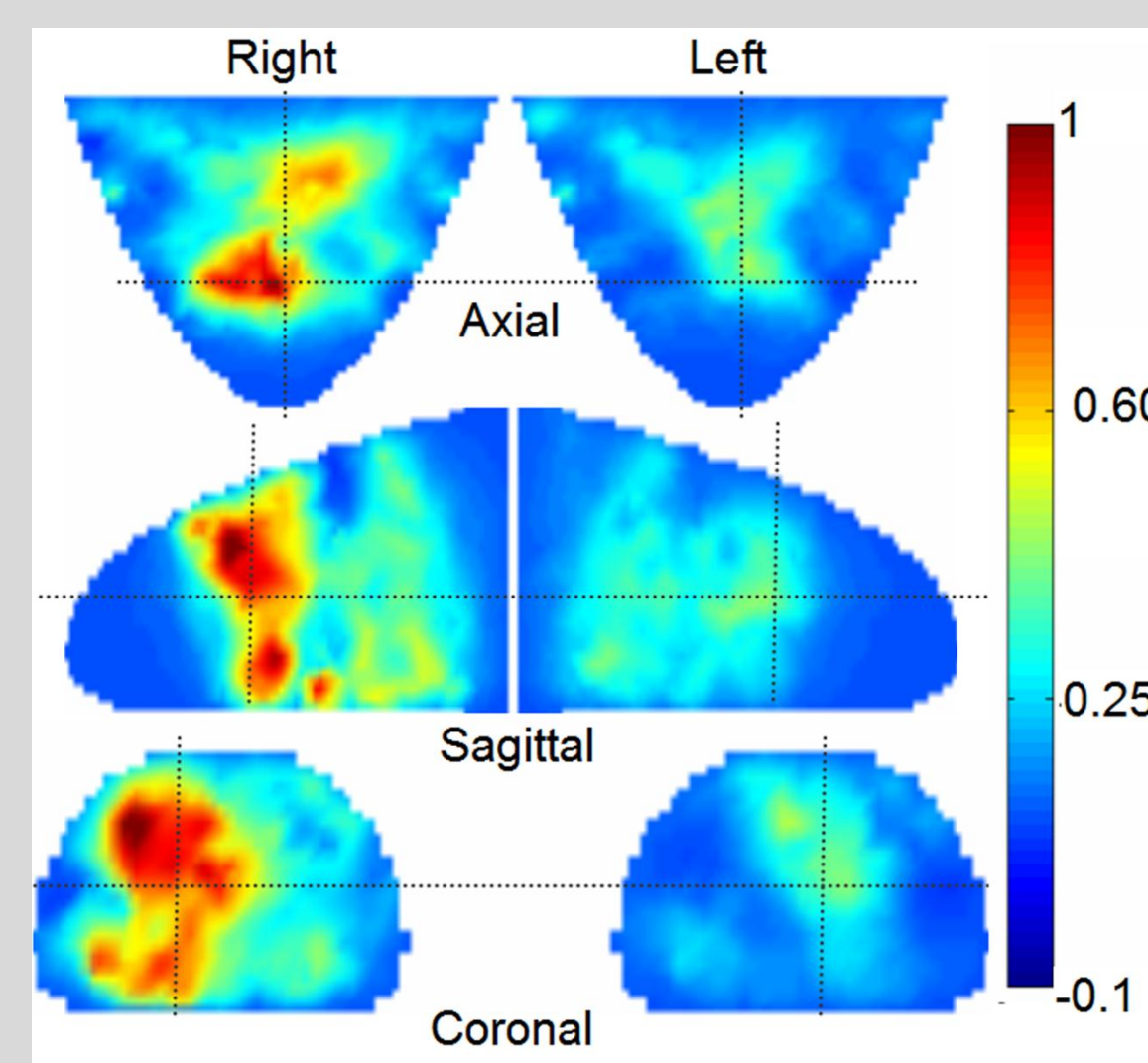## INDIVIDUAL Hb SIGNAL COMPONENT RESULTS (cont.)

Fig. 8. Orthogonal 2D sections of 3D reconstructed image of HbT stress-relaxation response (Hb concentrations are normalized to the maximum value), for a 40 y/o subject with a 6-cm IC in the right breast, following a full-compression protocol. (Similar findings are obtained for all components of the Hb signal and all compression-protocol variants.) A substantially larger response is seen in the affected breast, and the position of the maximum correlates well with the known tumor location. However, the image contrast and resolution are low.

Results in Figs. 6-8 show that the articulation-based fNIRS imaging data do contain the necessary diagnostic information. But we need a way to increase the discriminatory power. Consequently…

Fig. 9: Computation of the inter-breast Mahalanobis distance (MD) [5]. (a) Scatterplots (each dot represents one image pixel) of two Hb-signal components (HbSat and HbT in these examples) reveal that they tend to co-vary. Thus we seek to incorporate both of them into a single index. (b) In this rotated and rescaled representation of the scatterplots, the MD for each data point is the distance from the point to the origin.
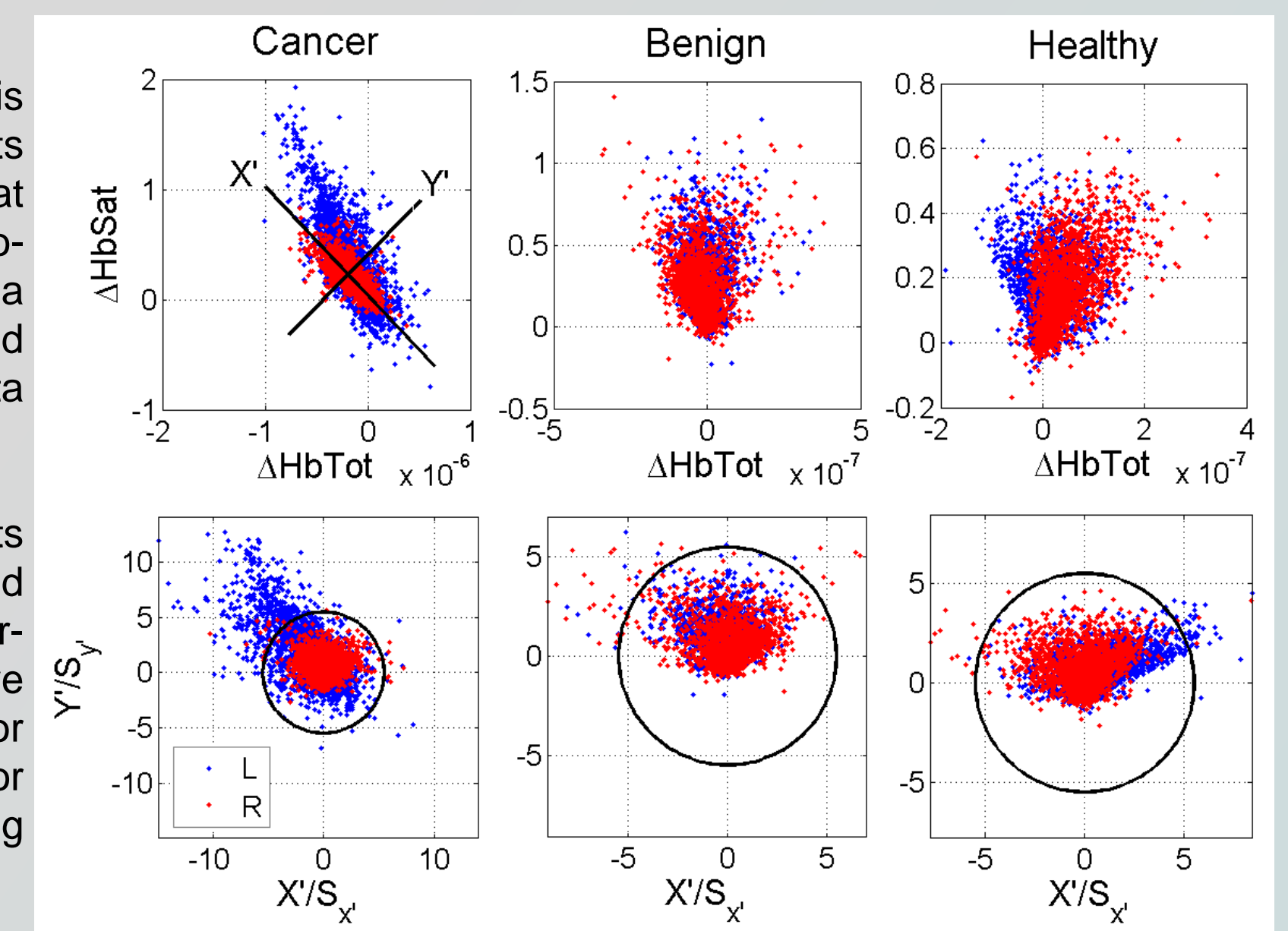
Empirically, we find that approximately 1% of data points have MD > 5.5 (black circles in (b)), for both healthy and affected breasts. But for cancer subjects, the inter-breast contrast is substantially increased when we modify the MD computation by referencing the data for one breast to the mean and covariance estimates for the contralateral breast, as indicated in the following formula:

$$MD_{breast1} = \sqrt{\left(x_{breast1} - \bar{x}_{breast2}\right)^T \left(C_{breast2}\right)^{-1} \left(x_{breast1} - \bar{x}_{breast2}\right)} \qquad (1)$$

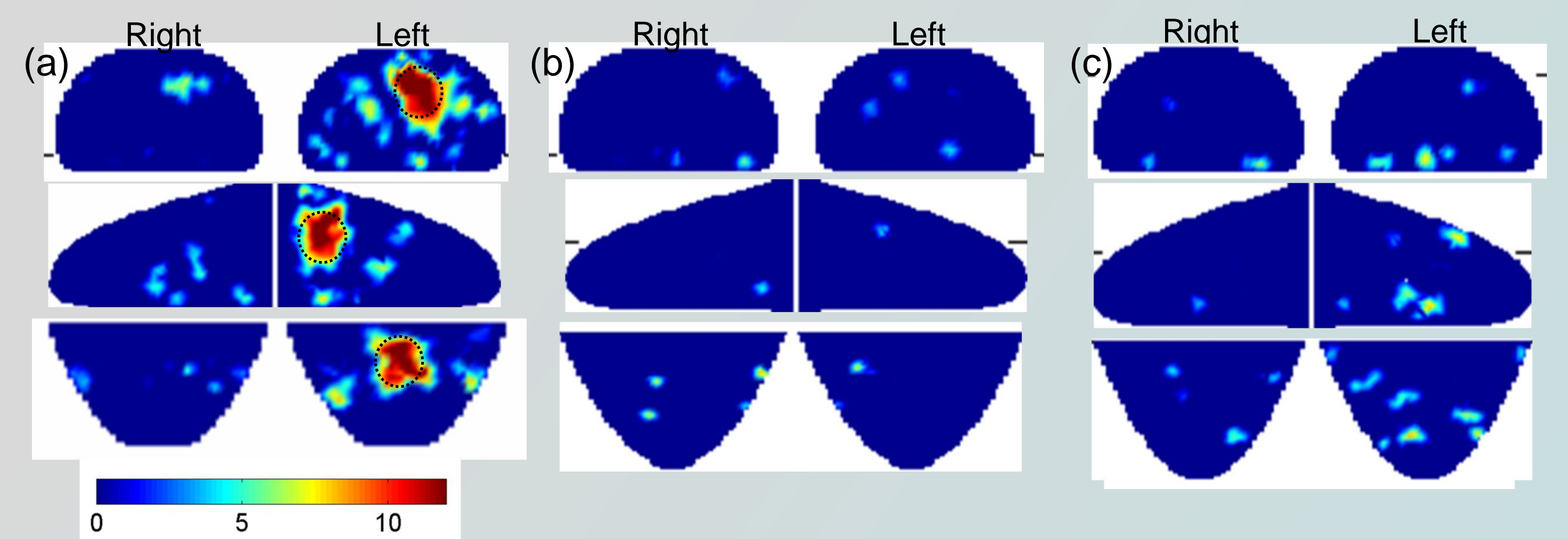## MAHALANOBIS DISTANCE-BASED RESULTS

Fig. 10. Orthogonal 2D sections (from top to bottom: coronal, sagittal and axial) of 3D spatial maps of the MD calculated using Eq. (1). To emphasize large-MD features, images are thresholded to show only regions with MD > 5.5. While similar results are obtained for all pairings of Hb-signal components, the images shown are MDs derived from the (HbT,HbD) pair. From data collected during stress relaxation following a 4.4-N ML compression. (a) Subject with breast cancer: 50 y/o, size D breasts, BMI = 44, and a 4-cm invasive ductal carcinoma in the left breast. Dotted black circles indicate that the tumor size and location, as determined from surgical and conventional imaging procedures, closely agree with the regions of highest MD values. (b) Subject with non-cancer breast pathology: 67 y/o, size D breasts, BMI = 30, and a 4-cm fibroadenoma in the right breast. (c) Healthy-control subject: 58 y/o, size D breasts, BMI = 31.
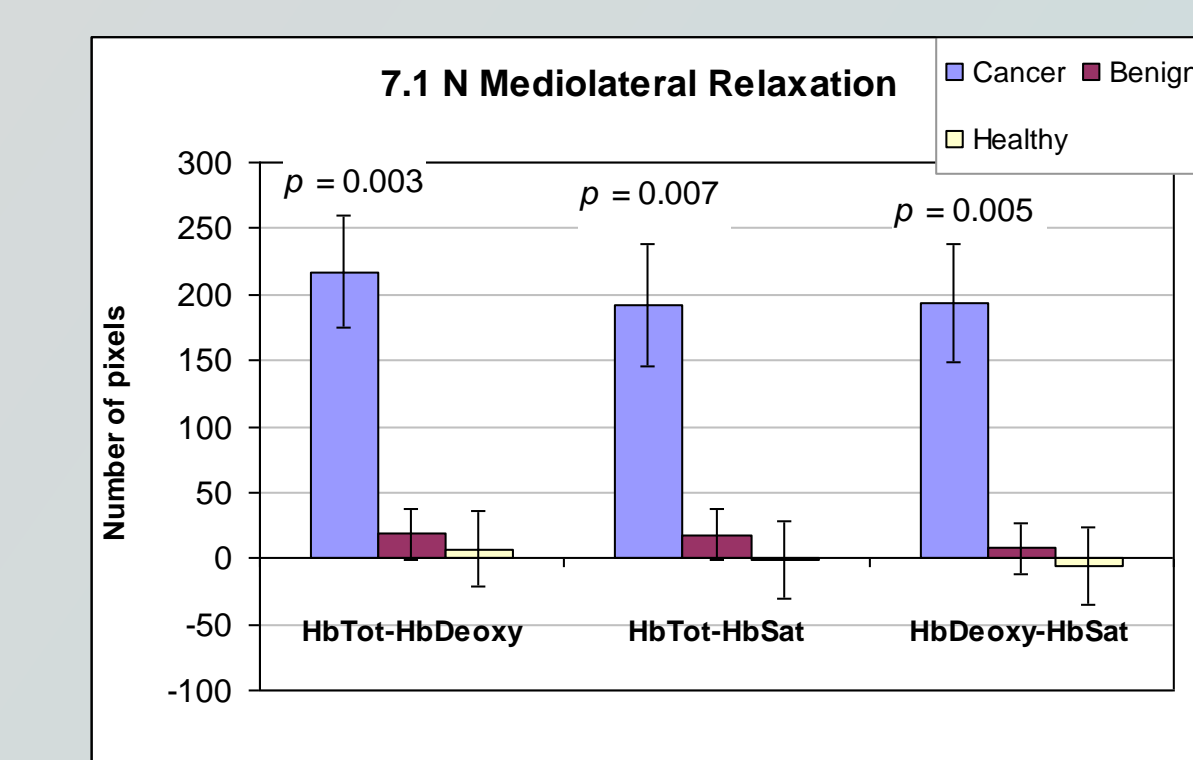

Fig. 11. Group means (colored bars) and standard errors (error bars) of the paired differences between the numbers of pixels that have MD greater than 5.5 in each breast. The paired difference results shown were computed from data collected during stress relaxation following a 7.1-N ML compression. Comparable results are obtained for MDs calculated from the (HbT,HbD), (HbT,HbSat), and (HbD,HbSat) Hb signal-component pairs. In each case the breast-cancer group mean is larger than that for the other two groups by a statistically highly significant amount. The MD index (cf. Fig. 7) does allow for accurate diagnostic decisions at the individual-subject level (see Table 2).
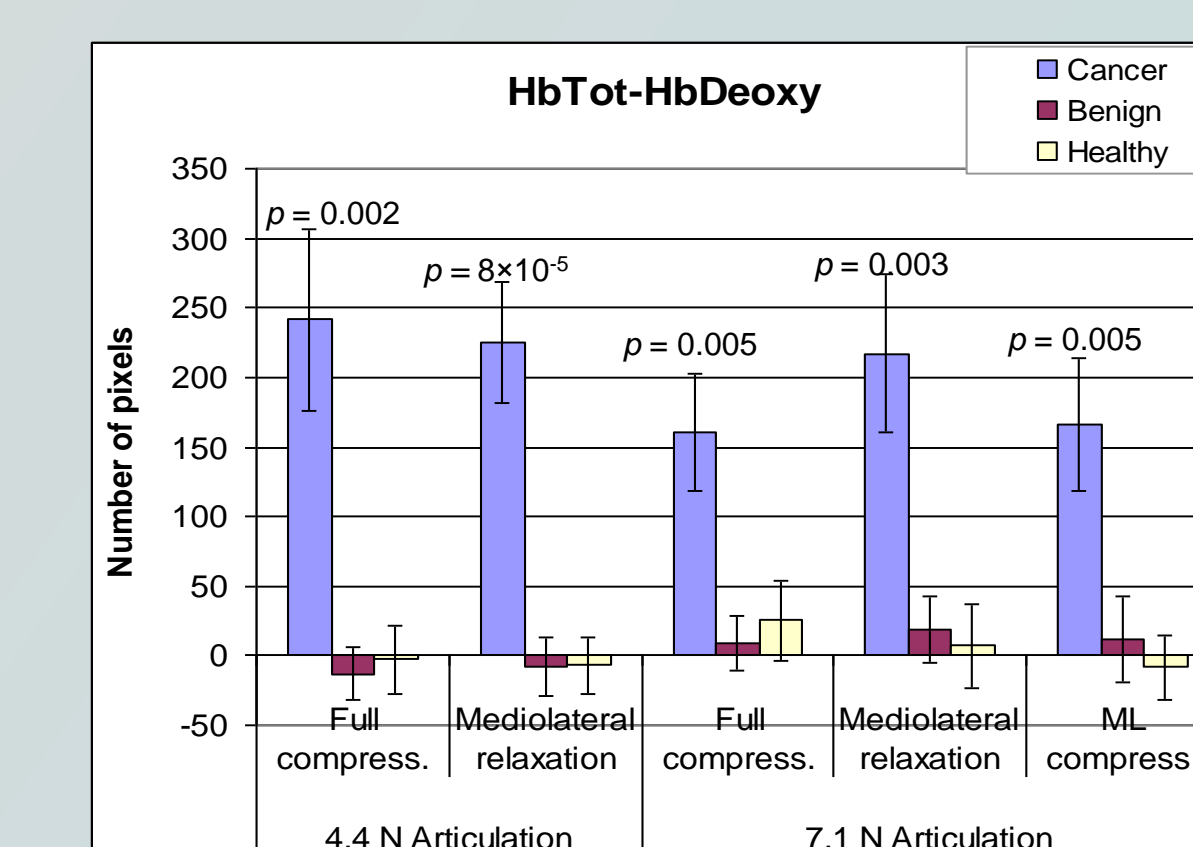

Fig. 12. Group means (colored bars) and standard errors (error bars) of the paired differences between the numbers of pixels that have MD greater than 5.5 in each breast. The paired difference results shown were computed from data collected during the stress relaxations (see Fig. 3) following 4.4-N full compression (i.e., compression using all AEs (see Fig.2)), 7.1-N full compression, and 7.1-N ML compression, and during the stress recoveries (see Fig. 3) following 4.4-N ML unloading and 7.1-N ML unloading. The MDs were calculated from the (HbT,HbD) Hb signal-component pair (comparable results are obtained for the other pairings). Statistically highly significant differences ($p < 0.01$) were found between the breast-cancer group and the other groups in all instances. The MD index (cf. Fig. 7) does allow for accurate diagnostic decisions at the individual-subject level (see Table 2).

Time Interval	AUC (%)	Std. Error	Asymptotic Significance	95% Confidence Interval for the AUC (%)	
4.4N_Full_Comp	82.4	0.067	< 0.001	69.4	95.5
4.4N_ML_Relax	89.8	0.044	< 0.001	81.1	98.5
7.1N_Full_Comp	78.7	0.063	0.001	66.4	91.0
7.1N_ML_Relax	82.1	0.059	< 0.001	70.5	93.6
7.1N_ML_Comp	78.1	0.070	0.001	64.4	91.8

Table 2. Receiver operator characteristic analysis [6] of the paired differences between the number of pixels that have MD larger than 5.5 in each breast (see Fig. 12). The AUC (i.e., area under curve) metric is the percentage of subjects who are correctly identified as belonging to either the cancer or "other" (i.e., having either a benign pathology or none) group. It is seen that the best result is found in the case of the most mild perturbation of the breast, in terms of applied-stress magnitude and the number of AEs deployed. This outcome is unsurprising if, in absolute terms, the differences between the mechanical properties of healthy and diseased tissues are small in comparison to their averages. In that case it would be expected that all breasts would respond in a more similar manner to a strong perturbation, while a milder one would better distinguish them.

CONCLUSION

Results presented show controlled articulation maneuvers can improve image contrast between breast tumors and both the surrounding healthy tissue and the contralateral breast. Breast-cancer diagnostic power is thereby improved.

References
[1] P. Vaupel, in Tumor Blood Flow (Springer, 2000), 41-45.
[2] R. Al abdi et al., Poster BSu3A.92 at Biomedical Optics and Digital Holography and Three-Dimensional Imaging (Miami, FL, April 29 - May 2, 2012).
[3] R. Al abdi et al., J. Optical Society of America A 28, 2473-2493 (2011).
[4] Y. Pei et al., Applied Optics 40, 5755-5769 (2001).
[5] R. De Maesschalck et al., Chemometrics and Intelligent Laboratory Systems 50, 1-18 (2000).
[6] C.E. Metz, Seminars in Nuclear Medicine 8, 283-298 (1978)